

Chiral Stoner magnetism in Dirac bands

Zhiyu Dong, Leonid Levitov¹

¹*Department of Physics, Massachusetts Institute of Technology, Cambridge, MA 02139*

We argue that Stoner magnetism in bands endowed with Berry curvature is profoundly influenced by the chiral interaction between Berry's orbital magnetization and spin chirality density. The key effect is that carriers moving in the presence of a spin texture see it as a source of a pseudo-magnetic field coupled to their orbital motion through a chiral Aharonov-Bohm effect. This interaction favors chiral spin textures such as skyrmions—the topologically protected objects with particle-like properties, stabilized in the ground state. The chiral interaction softens the threshold for Stoner instability, rendering chiral spin-ordered phases readily accessible under realistic conditions. We illustrate this effect for a graphene multilayer model, with magnetization and pseudo-magnetic fields taking different values in different valleys, yet the results are applicable to generic Stoner magnets.

The question of how Berry curvature impacts the many-body physics gained much attention with the advent of flat-band systems that host both topological bands and strong interactions. Such are, e.g., graphene multilayers, including moiré graphene[1–7] and field-biased non-moiré bilayers and trilayers [8–12]. New exotic orders appear when the moiré twist angle is tuned to a magic value [14] or when bands are flattened by a transverse electric field [13]. The richness of the observed orders, which include isospin (spin and valley) polarized phases coexisting with insulating and superconducting phases, motivates seeking new exotic orders.

Of special interest are the chiral itinerant magnetic phases, wherein spins wrap around the Bloch sphere, spanning a solid angle. Chiral spin textures have been explored in various magnetic systems[16, 17]. Famously, the Dzyaloshinskii-Moriya (DM) coupling favors spin textures[18] such as helical spin density waves [20–22] and skyrmions—the seminal topologically-protected particle-like spin configurations[19]. Is it possible to achieve a chiral spin order in graphene-based systems? At first sight, this may seem problematic as staple interactions that stabilize chiral magnetic orders are absent or extremely weak in graphene. Indeed, in noncentrosymmetric magnets—the bulk chiral magnetic metals[23–28] and magnetic layers[29, 30]—skyrmions are stabilized by the DM coupling governed by the microscopic spin-orbit interactions (SOI)[16, 18]. However, the microscopic SOI in graphene is usually negligible compared to other energy scales[31]. Likewise, the mechanisms that utilize frustration[32–34] are not found in graphene systems.

In this paper, we address this challenge by demonstrating a new mechanism that favors chiral spin orders. Namely, we show that chiral interactions that can drive chiral spin orders are naturally present in interacting electronic systems with bands that are equipped with Berry curvature. Unlike the mechanisms studied before, our chiral interactions do not require any extra broken symmetries, microscopic SOI or frustrations.

Specifically we argue that the exchange interaction in Dirac bands such as those found in graphene multilayers, moiré [1, 14, 35] and non-moiré[13, 15], results in a chiral interaction which leads to Stoner instability to-

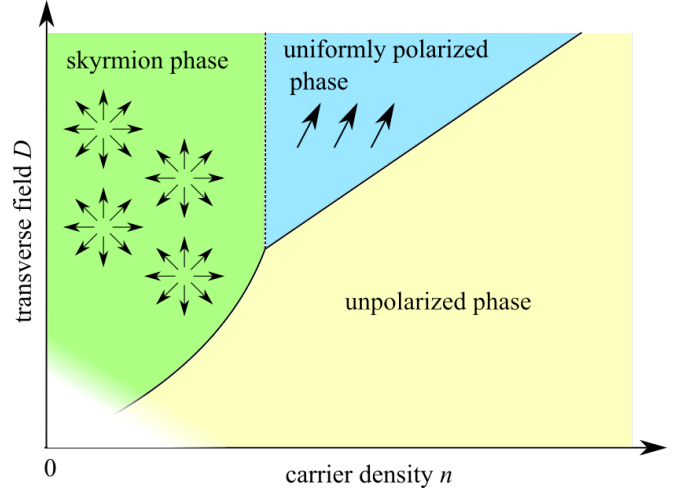


FIG. 1: The mean-field phase diagram for chiral magnetic order in the quadratic Dirac model, Eqs.(3) and (4), away from charge neutrality at $D = 0$. Transition between uniformly spin-polarized and unpolarized phases is first-order, occurring on a straight line in the n - D plane given by Eq.(16). Transition between skyrmion phase and uniformly polarized phase is second-order, with skyrmion density vanishing at the phase boundary given by Eq.(24). Here we ignore valley ordering, focusing on spin polarization in one valley (see text).

wards chiral ordered states. Fig.1 illustrates this for a quadratic Dirac band model of a field-biased bilayer graphene (BBG). The chiral interaction that drives this ordering arises from orbital magnetization due to k -space Berry curvature of Dirac carriers. This interaction occurs in the presence of a position-dependent spin polarization, taking the form:

$$\delta F = \int d^2x \sum_i -(M_{i,+} - M_{i,-})B_i(\mathbf{x}), \quad (1)$$

where $M_{i,\pm}$ is the orbital magnetization of the majority-spin and minority-spin carriers (see Eq.(10)). The quantity $B_i(\mathbf{x})$ is defined as the topological density of spin texture multiplied by the flux quantum ϕ_0 :

$$B_i(\mathbf{x}) = \frac{\phi_0}{4\pi} \mathbf{S}_i \cdot (\partial_1 \mathbf{S}_i \times \partial_2 \mathbf{S}_i), \quad \phi_0 = hc/e, \quad (2)$$

where $\mathbf{S}_i(\mathbf{x})$ is the unit-vector field representing spin polarization of carriers in valleys $i = K, K'$. The quantity $B_i(\mathbf{x})$ represents a ‘magnetic field’ associated with the spin-dependent (chiral) Aharonov-Bohm effect.

The key aspect of the chiral interaction, Eq.(1), is that the position-dependent quantization axis along which carrier spins are polarized is, in general, allowed to twist in space. Eq.(1), derived below, can be viewed as an extension of the basic electromagnetic coupling of a magnetic moment and external field, $E = -\mathbf{M} \cdot \mathbf{B}$.

Since M_i describes orbital magnetization whereas B_i is a property of spin texture, the interaction in Eq.1 resembles the atomic spin-orbital interaction (SOI) $E \sim \mathbf{L} \cdot \mathbf{S}$. Yet, the interaction in Eq.1 is of a totally different origin, governed by the interplay of momentum-space Berry curvature and exchange interaction, not relying on spin-orbital coupling. It therefore has unique symmetry properties distinct from those of SOI: the quantities B_i are invariant under the $SU(2)$ spin rotations performed separately in each valley, which leave the orbital quantities $M_{i,\pm}$ intact. As discussed below, the interaction in Eq.1 also respects discrete symmetries of BBG, including the time-reversal and mirror symmetries.

We note that the chiral interaction that drives skyrmions in our theory is essentially different from the one described in recent works, where skyrmions in isospin-polarized moiré graphene flat bands have been invoked to predict exotic superconductivity [36, 37]. The mechanism that stabilizes skyrmions in these papers is an isospin extension of quantum Hall ferromagnet physics, in which the skyrmion emerge in Landau levels spin-split by exchange interactions [17, 38–40]. Skyrmions of this type have been predicted [41, 42] and recently observed [43, 44] in graphene at high magnetic fields.

Next, we derive the interaction between spin-chirality and orbital magnetization, Eq.(1), by a microscopic analysis starting from a fully $SU(2)$ -invariant Hamiltonian not involving SOI. To that end, we consider Stoner magnetism of Dirac fermions with spin-exchange coupling

$$\mathcal{H} = \sum_p c_p^\dagger H(p) c_p - \frac{1}{2} \sum_{\mathbf{x}, \mathbf{x}'} U(\mathbf{x} - \mathbf{x}') : s_\alpha(\mathbf{x}) s_\alpha(\mathbf{x}') :, \quad (3)$$

where the last term is an exchange interaction written in terms of spin density $s_\alpha(\mathbf{x}) = \psi^\dagger(\mathbf{x}) \sigma_\alpha \psi(\mathbf{x})$ with Pauli matrices σ_α representing ordinary spin-1/2 variables, $\alpha = 1, 2, 3$. The density-density interaction $e^2/\kappa|r - r'|$, which generates the exchange interaction on a microscale, is suppressed for conciseness. Its role will be discussed below. Here we will use a toy-model form of exchange coupling $U(\mathbf{x} - \mathbf{x}') = 2\pi U_0 \xi^{-2} e^{-(\mathbf{x} - \mathbf{x}')^2/2\xi^2}$, normalized so that $\int d^2x U(\mathbf{x}) = U_0$. The Dirac band is described by a general 2×2 Dirac Hamiltonian in the sublattice A, B basis. Here we consider the quadratic Dirac problem

$$H(p) = \begin{pmatrix} D & \frac{(p_1 - i\eta p_2)^2}{2m} \\ \frac{(p_1 + i\eta p_2)^2}{2m} & -D \end{pmatrix} \quad (4)$$

with $\eta = \pm 1$ for the valleys K and K' , respectively. Accordingly, the quantities $\psi(\mathbf{x})$, $\psi^\dagger(\mathbf{x})$, c_p , c_p^\dagger are spinors with the A and B sublattice components and the ordinary spin-1/2 components. The Hamiltonian $H(p)$ is particle-hole symmetric, with the terms producing particle-hole asymmetry and trigonal warping ignored for simplicity. Incorporating these terms later or generalizing to other Dirac band types would be straightforward. Realistic parameter values are discussed beneath Eq.(24).

To describe spin textures, we perform a mean-field analysis in which the field describing magnetic order is allowed to vary in space. Since the exchange interactions are predominantly intravalley it will be sufficient to carry out the analysis for an individual valley and consider the role of valley degrees of freedom later. The Hubbard-Stratonovich (HS) transformation is carried out using an ordering field $\mathbf{h}(\mathbf{x})$ with both the modulus and orientation being position-dependent, $e^{\int dt \sum_k \frac{U(k)}{2} \mathbf{s}_k \cdot \mathbf{s}_{-k}} = \int D[\mathbf{h}] e^{\int dt \sum_k \mathbf{h}_k(t) \cdot \mathbf{s}_{-k} - \frac{\mathbf{h}_k(t) \cdot \mathbf{h}_{-k}(t)}{2U(k)}}$, where $D[\mathbf{h}] = \prod_{k,t} d\mathbf{h}_k(t)$. Here we introduced Fourier harmonics of the HS field, the spin density and the interaction $\mathbf{h}_k = \int d^2x \mathbf{h}(\mathbf{x}) e^{-i\mathbf{k}\mathbf{x}}$, $\mathbf{s}_k = \int d^2x \mathbf{s}(\mathbf{x}) e^{-i\mathbf{k}\mathbf{x}}$, $U(k) = \int d^2x U(\mathbf{x}) e^{-i\mathbf{k}\mathbf{x}} = U_0 e^{-k^2 \xi^2/2}$. Integrating out fermions and assuming a time-independent $\mathbf{h}(\mathbf{x})$, we obtain the free energy with a nonlocal $h(\mathbf{x})h(\mathbf{x}')$ interaction

$$F = \text{Tr} \log [i\omega - H(p) - h_\alpha(\mathbf{x}) \sigma_\alpha] + \sum_k \frac{\mathbf{h}_k \cdot \mathbf{h}_{-k}}{2U(k)}, \quad (5)$$

where, for conciseness, the chemical potential μ is incorporated in H and Tr denotes $\sum_x \int \frac{d\omega d^2p}{(2\pi)^3} \text{Tr}_{2 \times 2}$. In this case, it is easy to compare the states with uniform polarization and those with spatially dependent $\mathbf{h}(\mathbf{x})$ on equal footing. The saddle point condition yields a time-independent $h = |\mathbf{h}|$, which is nothing but the Stoner mean field value

$$h = U_0(n_+ - n_-)/2, \quad (6)$$

where n_+ and n_- are local densities of carriers with spins parallel and antiparallel to local spin quantization axis $\mathbf{h}(\mathbf{x})$. We will call these spin species the majority and the minority spins, respectively. When the system is fully polarized, the mean field equals $h = U_0 n/2$. The term $-h_\alpha(\mathbf{x}) \sigma_\alpha$ describes electron spins coupled to a spin texture with a position-dependent magnetization polarized along the unit vector $\mathbf{S}(\mathbf{x}) = \mathbf{h}(\mathbf{x})/h$, where $|\mathbf{h}(\mathbf{x})| = h$.

Accordingly, we consider the last term in free energy [Eq.(5)] $F_h = \sum_k \frac{\mathbf{h}_k \cdot \mathbf{h}_{-k}}{2U(k)}$ assuming that the local spin-quantization axis is slowly-varying, $\xi \partial_\mu S_\alpha \ll 1$. Assuming that the exchange interaction radius ξ exceeds the Fermi wavelength, which makes the short-wavelength fluctuations in $\mathbf{h}(\mathbf{x})$ weak, we can approximate $U(k)^{-1} = U_0^{-1}(1 + k^2 \xi^2/2)$, giving

$$F_h = \sum_k \frac{\mathbf{h}_k \cdot \mathbf{h}_{-k}}{2U(k)} \approx \sum_x \frac{h^2}{2U_0} + \frac{1}{2} J (\partial_\mu S_\alpha)^2, \quad (7)$$

with the spin stiffness parameter defined as $J = \frac{\xi^2 h^2}{2U_0}$.

Next, we introduce a gauge field describing Berry phase for electrons in the presence of a slowly varying spin texture[45–48]. This is done by carrying out spin rotation at every point in position space, $|\mathbf{S}(x)\pm\rangle = U_{\mathbf{S}(x)}|z\pm\rangle$, such that $\mathbf{h}_\alpha \sigma_\alpha = U_{\mathbf{S}(x)}^\dagger h \sigma_3 U_{\mathbf{S}(x)}$. Absorbing μ in $H(p)$, we have

$$F = \int d^2x \sum_{\omega,p} \text{Tr} \log [\omega - H(\mathbf{p} - \mathbf{a}\sigma_3) - h\sigma_3] + F_h \quad (8)$$

where F_h is defined in Eq.(7). The gauge field \mathbf{a} describing position-dependent spin rotation is defined as $a_\mu(x) = -\frac{i}{2} \text{Tr}(\sigma_z U_{\mathbf{S}(x)}^{-1} \partial_\mu U_{\mathbf{S}(x)})$ [49–51]. The quantity $\nabla \times \mathbf{a}$ is nothing but the spin chirality density, since

$$\nabla \times \mathbf{a} = \frac{1}{2} \epsilon_{\mu\nu} \mathbf{S} \cdot (\partial_\mu \mathbf{S} \times \partial_\nu \mathbf{S}). \quad (9)$$

This relation links the skyrmion topological density and the pseudomagnetic field, Eq.(2). For a derivation of this result, which follows closely previous literature, see [54].

We are interested in the instability of a spatially-uniform magnetic order towards a twisted state with a nonzero gauge field \mathbf{a} . We therefore consider power-series expansion of the electronic energy in Eq.(8) in small \mathbf{a} . We neglect the longitudinal fluctuations of \mathbf{h} , which are gapped, focusing on the soft angular fluctuations, $\delta\mathbf{h}(\mathbf{x}) \perp \mathbf{h}$. For a slowly varying unit-vector field $\mathbf{S}(\mathbf{x}) = \mathbf{h}/|\mathbf{h}|$, the dependence on \mathbf{a} in the first term of Eq.(8), hereafter referred to as F_1 , can be found by an expansion in powers of \mathbf{a} . At order \mathbf{a}^2 we have

$$F_1 = \sum_{\pm} E_{\pm} - \Delta M B + \frac{1}{2} \chi B^2, \quad \Delta M = M_+ - M_-,$$

$$E_{\pm} = \sum_k (\epsilon_k^{\pm} - \mu) f(\epsilon_k^{\pm}), \quad \chi = \chi_+ + \chi_-. \quad (10)$$

where the quantities M_{\pm} and χ_{\pm} are the orbital magnetizations and the Landau diamagnetic susceptibility of the majority and minority spins, $B(\mathbf{x}) = \frac{e}{h} \nabla \times \mathbf{a}$ is the pseudo magnetic field. Using the relation in Eq.(9), it is straightforward to show that B defined in this way is identical to B given in Eq.(2). The E_{\pm} contributions are the energies of spin-majority and spin-minority fermions in the bands with an exchange spin splitting, $\epsilon_k^s = \epsilon_k \mp h$, evaluated at $\mathbf{a} = 0$, whereas the second and third terms represent the dependence on the pseudomagnetic field $\nabla \times \mathbf{a}$ at second order in \mathbf{a} .

The contributions $\mp M_{\pm} B$ describe orbital magnetization of spin-majority and spin-minority carriers, arising due to Berry curvature, coupled to the pseudomagnetic field. Crucially, both the conduction and valence bands contribute to M . Therefore, perhaps counterintuitively, both up-spin and down-spin contributions to M matter even if the conduction band is fully polarized. The values M_{\pm} depend on the band filling and will be discussed below. The sign \mp accounts for the fact that the Berry

phase for the carriers with opposite spins, moving in a slowly varying texture $\mathbf{h}(\mathbf{x})$, has opposite signs, described by the σ_3 factor in Eq.(8). In this form, Eq.(8) describes the limit of a weak, non-quantizing pseudomagnetic field B , which is sufficient for the purpose of analyzing the transition from zero to nonzero B .

Putting everything together, we can write the system energy in the absence of pseudo magnetic field B as

$$F = \int d^2x \left[E_+ + E_- + \frac{h^2}{2U_0} + \frac{J}{2} (\partial_\mu \mathbf{S})^2 \right] \quad (11)$$

Using this expression, we can seek the ground state by comparing the energies of the ordered and disorder states. To account for the effect of a long-range $1/r$ density-density interaction without incorporating it explicitly in the mean-field analysis, we consider different states at the same total carrier density n . This approach is valid due to the large charging energy values $E_c = \frac{1}{2} V_0 n^2$ which typically exceed other energy scales in the system. When E_c is included in the analysis, the dependence of the total energy on n is dominated by the following terms:

$$\frac{V_0 n^2}{2} - \mu n = \frac{V_0}{2} \left(n - \frac{\mu}{V_0} \right)^2 - \frac{\mu^2}{2V_0} \quad (12)$$

These terms pin the density to $n = \frac{\mu}{V_0}$ regardless of the order type. Therefore, comparing energies of different states at the same μ in the presence of E_c is equivalent to comparing their energies at the same n .

To analyze the ordering described by Eq.(11) we proceed in two steps: First analyze the Stoner instability while temporarily ignoring B . Next, we consider the dependence on B and the transition from a uniform magnetic order to a twisting order.

In the absence of B , Eq.(11) describes the standard Stoner instability—a transition from a disordered state to a uniformly polarized state. Since the density of states in the quadratic Dirac band monotonically decreases as a function of energy, the ground state configuration is either fully spin polarized or spin unpolarized, depending on the band parameters and interaction strength. [For a more general band dispersion partial spin polarization can also occur.] The energy density of a fully polarized phase where $n_+ = n, n_- = 0$ is given by

$$F_{\text{fp}} = E_{\text{tot}}(n) - \frac{U_0 n^2}{2} \quad (13)$$

where n is a given total carrier density. We have used Eq.(6). Here $E_{\text{tot}}(n) = \int_0^{\sqrt{4\pi n}} \frac{d^2 k}{4\pi^2} \epsilon_k$ represents the total kinetic energy of electrons of density n in one spin one valley in the absence of interaction. Similarly, the energy of unpolarized state where $n_+ = n_- = n/2$ is given by

$$F_{\text{unp}} = 2E_{\text{tot}}(n/2) \quad (14)$$

Here, we have used $h = 0$ in unpolarized phase. For our quadratic Dirac band, E_{tot} takes the following form:

$$E_{\text{tot}}(n) = \frac{mD^2}{4\pi} \left(\log(x + \sqrt{1+x^2}) + x\sqrt{1+x^2} \right), \quad (15)$$

where $x = \frac{2\pi n}{mD}$ is a dimensionless density parameter. The regime of interest is that of strong exchange interaction, which corresponds to low values $n \ll 2mD$. In this case, we can use power-series expansion $E_{\text{tot}}(n) = \frac{mD^2}{2\pi}(x + \frac{5}{12}x^3 + \dots)$. This allows a direct comparison of the energies of polarized and unpolarized states. Simple algebra then predicts the fully polarized state to win when

$$\frac{n}{D} < \frac{2m^2U_0}{5\pi^2}. \quad (16)$$

Therefore, the phase boundary is a straight line on the D - n phase diagram (see Fig.1). This phase transition is first-ordered since the full polarization occurs abruptly.

Next, we consider the role of a spin texture $\mathbf{S}(\mathbf{x})$ and derive the condition for skyrmion proliferation. From Eqs.(10),(11), we see that system energy depends on \mathbf{S} as $E_{\mathbf{S}} = \int d^2x \left[\frac{J}{2}(\partial_\mu S_\alpha)^2 \mp \Delta M B + \frac{\chi}{2}B^2 \right]$. Therefore, the spin texture enters the energetics in two ways: through pseudo magnetic field B which is proportional to the spin chirality density Eq.(9), and also through the spin stiffness energy $\frac{J}{2}(\partial_\mu \mathbf{S})^2$. However, the latter contribution has a lower bound associated with spin chirality

$$\frac{1}{2} \int d^2x (\partial_\mu \mathbf{S})^2 \geq \frac{1}{2} \int d^2x |\epsilon_{\mu\nu} \mathbf{S} \cdot (\partial_\mu \mathbf{S} \times \partial_\nu \mathbf{S})|.$$

This relation follows from the well-known identity[19]:

$$\int d^2x [(\partial_\mu \mathbf{S})^2 \mp \epsilon_{\mu\nu} \mathbf{S} \cdot (\partial_\mu \mathbf{S} \times \partial_\nu \mathbf{S})] \quad (17)$$

$$= \frac{1}{2} \int d^2x (\partial_\mu \mathbf{S} \pm \epsilon_{\mu\nu} \mathbf{S} \times \partial_\nu \mathbf{S})^2 \geq 0, \quad (18)$$

Expressing the stiffness energy through $|B|$ gives

$$E_{\mathbf{S}}[B] = \int d^2x \left[-\Delta M B + \frac{2Je}{\hbar c} |B| + \frac{\chi}{2} B^2 \right], \quad (19)$$

Obviously, the quantity $E_{\mathbf{S}}[B]$ is only well-defined when spin polarization occurs. Therefore, below we focus on the effect of $E_{\mathbf{S}}[B]$ on the fully spin-polarized state.

It is now straightforward to derive the condition for nonzero chirality to be favored. The free energy in Eq.(19) gives the threshold for nucleating chiral spin textures in the ground state:

$$\Delta M \geq 2Je/\hbar c. \quad (20)$$

As a reminder, $\Delta M = M_+ - M_-$, $M_\pm = M(\mu \pm h)$ in one particular valley. Below, without loss of generality, we focus on K valley. In our particle-hole-symmetric Dirac model, the total orbital magnetization of all electrons in valley K takes a simple form[52–54]:

$$M_K(\mu) = \begin{cases} \frac{eD}{2\pi\hbar}, & \mu > D \\ \frac{e\mu}{2\pi\hbar}, & -D < \mu < D \\ -\frac{eD}{2\pi\hbar}, & \mu < -D \end{cases}, \quad (21)$$

taking opposite values in valleys K and K' . This dependence, with M being constant in each band, is a unique

property of our Dirac band[54]. A more general model would yield M that depends on doping in each band.

For a fully polarized state at a carrier density n , $M_+ = \frac{eD}{2\pi\hbar}$ whereas M_- depends on density. To calculate M_- we first calculate chemical potential using $\mu + h = \sqrt{D^2 + (\frac{4\pi n}{2m})^2}$ which gives:

$$\mu = \sqrt{D^2 + (2\pi n/m)^2} - U_0 n/2 \sim D - U_0 n/2 \quad (22)$$

where we have ignored $O(n^2)$ terms since we are interested in the low density regime. Plugging this into Eq.(21) we find

$$M_- = M(\mu - h) = (D - U_0 n) e/2\pi\hbar \quad (23)$$

As a result, $\Delta M = eU_0 n/(2\pi\hbar)$. Plugging this into Eq.(20) and using $J = \frac{\xi^2 \hbar^2}{2U_0}$, we find a transition from fully polarized state to chiral spin state occurs at $\frac{eU_0 n}{2\pi\hbar} \geq \frac{\xi^2 U_0 n^2 e}{4\hbar}$ which gives

$$n\xi^2 \leq \frac{2}{\pi} \quad (24)$$

Since our mean-field analysis works for ξ exceeding the Fermi wavelength λ_F , the condition in Eq.(24) is marginally met. The threshold Eq.(24) can be further softened in multilayer graphene (such as tlayer, quadlayer, or pentalayer) because ΔM is proportional to the valley Chern number, which for N -layer graphene can take values that scale with the number of layers, $C = N/2$. As a result, the threshold softens to $n\xi^2 \leq \frac{2}{\pi} C$.

To show that the chiral phase is readily accessible we estimate the required size of ξ using realistic parameters. In BBG system of interest, the carrier density n_c at the onset of Stoner transition can be estimated from Eq.(16). For interaction strength $U_0 = 5 \times 10^3 \text{ meV nm}^2$, a band mass $m = 0.03m_e$ and a typical high value [8–12] $D = 100 \text{ meV}$, it predicts Stoner instability at $n_c \sim 3 \times 10^{11} \text{ cm}^{-2}$. Eq.(24) then predicts that to nucleate skyrmions the interaction radius must satisfy $\xi \lesssim 20 \text{ nm}$, a realistic value comparable to the Fermi wavelength.

A phase diagram describing the competition between the orders described above is shown in Fig.1. The transition line from uniformly polarized phase to skyrmion phase is given by Eq.(24). We note that, compared to the transition line between the uniformly polarized phase and unpolarized phase, the transition line between skyrmion phase and unpolarized phase is pushed slightly into the unpolarized phase. This is because when skyrmion condenses, the energy contribution from pseudo magnetic field Eq.(19) is always negative and tends to stabilize ordered state. This phase boundary is a first-order phase transition because the translation symmetry and the spin $SU(2)$ symmetry are simultaneously broken on this line.

We note that the condition for skyrmion instability Eq.(24) can be softened in Dirac bands with larger valley Chern numbers, since ΔM is proportional to the total Hall conductivity in the lower band. Large valley Chern

numbers can be achieved in graphene multilayers, such as trilayer, quadlayer, or pentalayer. Another appealing system is moiré graphene, where valley-Chern minibands [35] give rise to a doping-dependent orbital magnetization, potentially leading to a skyrmion instability triggered by spin polarization onset.

The proliferation of skyrmions through the mechanism discussed above can lead to two possible ground states—skyrmion crystal and skyrmion liquid, arising when zero-point or thermal fluctuations are weak and strong, respectively. These phases have properties similar to those of the vortex lattice and vortex liquid phases in superconductors [55–58]. Which of the two states wins in the true ground state is an interesting topic for future work.

These two phases can be readily distinguished by trans-

port measurements. In the presence of a valley polarization, which is ubiquitous in BBG and moiré graphene systems, we expect quantized topological Hall effect in both states in the absence of an applied magnetic field [51, 59]. When time-reversal is not spontaneously broken (no valley polarization), a quantized topological valley Hall effect will occur, since the time-reversal requires skyrmions in valley K and K' to have opposite chiralities. On the other hand, the longitudinal transport will be very different in the two phases—vanishing for skyrmion crystal and nonzero for skyrmion liquid, dual to that of superconducting vortex crystals and liquids.

This work greatly benefited from discussions with Eli Zeldov, Steven Kivelson and Patrick Lee.

-
- [1] Andrei, E.Y. and MacDonald, A.H., 2020. Graphene bilayers with a twist. *Nature materials*, 19(12), pp.1265-1275.
 - [2] Cao, Y., Fatemi, V., Fang, S., Watanabe, K., Taniguchi, T., Kaxiras, E. and Jarillo-Herrero, P., 2018. Unconventional superconductivity in magic-angle graphene superlattices. *Nature*, 556(7699), pp.43-50.
 - [3] Cao, Y., Fatemi, V., Demir, A., Fang, S., Tomarken, S.L., Luo, J.Y., Sanchez-Yamagishi, J.D., Watanabe, K., Taniguchi, T., Kaxiras, E. and Ashoori, R.C., 2018. Correlated insulator behaviour at half-filling in magic-angle graphene superlattices. *Nature*, 556(7699), pp.80-84.
 - [4] Cao, Y., Rodan-Legrain, D., Rubies-Bigorda, O., Park, J.M., Watanabe, K., Taniguchi, T. and Jarillo-Herrero, P., 2020. Tunable correlated states and spin-polarized phases in twisted bilayer-bilayer graphene. *Nature*, 583(7815), pp.215-220.
 - [5] Zondiner, U., Rozen, A., Rodan-Legrain, D., Cao, Y., Queiroz, R., Taniguchi, T., Watanabe, K., Oreg, Y., von Oppen, F., Stern, A. and Berg, E., 2020. Cascade of phase transitions and Dirac revivals in magic-angle graphene. *Nature*, 582(7811), pp.203-208.
 - [6] Wong, D., Nuckolls, K.P., Oh, M., Lian, B., Xie, Y., Jeon, S., Watanabe, K., Taniguchi, T., Bernevig, B.A. and Yazdani, A., 2020. Cascade of electronic transitions in magic-angle twisted bilayer graphene. *Nature*, 582(7811), pp.198-202.
 - [7] Saito, Y., Yang, F., Ge, J., Liu, X., Taniguchi, T., Watanabe, K., Li, J.I.A., Berg, E. and Young, A.F., 2021. Isospin Pomeranchuk effect in twisted bilayer graphene. *Nature*, 592(7853), pp.220-224.
 - [8] Seiler, A.M., Geisenhof, F.R., Winterer, F., Watanabe, K., Taniguchi, T., Xu, T., Zhang, F. and Weitz, R.T., 2021. Quantum cascade of new correlated phases in trigonally warped bilayer graphene. *arXiv preprint arXiv:2111.06413*.
 - [9] Zhou, H., Holleis, L., Saito, Y., Cohen, L., Huynh, W., Patterson, C.L., Yang, F., Taniguchi, T., Watanabe, K. and Young, A.F. Isospin magnetism and spin-polarized superconductivity in Bernal bilayer graphene. *Science*, 375(6582), pp.774-778 (2022).
 - [10] de la Barrera, S.C., Aronson, S., Zheng, Z., Watanabe, K., Taniguchi, T., Ma, Q., Jarillo-Herrero, P. and Ashoori, R., 2022. Cascade of isospin phase transitions in Bernal stacked bilayer graphene at zero magnetic field. *Nature Physics*, pp.1-5.
 - [11] Zhou, H., Xie, T., Taniguchi, T., Watanabe, K. and Young, A.F., 2021. Superconductivity in rhombohedral trilayer graphene. *Nature*, 598(7881), pp.434-438.
 - [12] Zhou, H., Xie, T., Ghazaryan, A., Holder, T., Ehrets, J.R., Spanton, E.M., Taniguchi, T., Watanabe, K., Berg, E., Serbyn, M. and Young, A.F., 2021. Half-and quarter-metals in rhombohedral trilayer graphene. *Nature*, 598(7881), pp.429-433.
 - [13] McCann, E. and Koshino, M., 2013. The electronic properties of bilayer graphene. *Reports on Progress in physics*, 76(5), p.056503.
 - [14] Bistritzer, R. and MacDonald, A.H., 2011. Moiré bands in twisted double-layer graphene. *Proceedings of the National Academy of Sciences*, 108(30), pp.12233-12237.
 - [15] Castro, E.V., Peres, N.M.R., Stauber, T. and Silva, N.A.P., Low-density ferromagnetism in biased bilayer graphene. *Phys. Rev. Lett.*, 100(18), 186803 (2008).
 - [16] A. Fert, N. Reyren, V. Cros, Magnetic skyrmions: advances in physics and potential applications, *Nature Reviews Materials*, 2, 17031 (2017)
 - [17] N. Nagaosa, Y. Tokura, Topological properties and dynamics of magnetic skyrmions. *Nature Nanotech* 8, 899-911 (2013).
 - [18] A. N. Bogdanov, U. K. Rössler, Chiral symmetry breaking in magnetic thin films and multilayers. *Phys. Rev. Lett.* 87, 037203 (2001).
 - [19] A. M. Polyakov, *Gauge Fields and Strings* (Harwood Acad. Publ. 1987).
 - [20] Binz, B., Vishwanath, A. and Aji, V., Theory of the helical spin crystal: a candidate for the partially ordered state of MnSi. *Phys. Review Lett.*, 96(20), 207202 (2006).
 - [21] Nakanishi, O., Yanase, A., Hasegawa, A. and Kataoka, M., 1980. The origin of the helical spin density wave in MnSi. *Solid State Communications*, 35(12), pp.995-998.
 - [22] Kataoka, M. and Nakanishi, O., 1981. Helical spin density wave due to antisymmetric exchange interaction. *Journal of the Physical Society of Japan*, 50(12), pp.3888-3896.
 - [23] Roessler, U.K., Bogdanov, A.N. and Pfeleiderer, C. Spontaneous skyrmion ground states in magnetic metals. *Nature*, 442(7104), pp.797-801 (2006).

- [24] Mühlbauer, S., Binz, B., Jonietz, F., Pfleiderer, C., Rosch, A., Neubauer, A., Georgii, R. and Böni, P., 2009. Skyrmion lattice in a chiral magnet. *Science*, 323(5916), pp.915-919.
- [25] Neubauer, A., Pfleiderer, C., Binz, B., Rosch, A., Ritz, R., Niklowitz, P.G. and Böni, P., Topological Hall effect in the A phase of MnSi. *Phys. Rev. Lett.*, 102(18), 186602 (2009).
- [26] Yu, X.Z., Onose, Y., Kanazawa, N., Park, J.H., Han, J.H., Matsui, Y., Nagaosa, N. and Tokura, Y. Real-space observation of a two-dimensional skyrmion crystal. *Nature*, 465(7300), pp.901-904. (2010)
- [27] Seki, S., Yu, X.Z., Ishiwata, S. and Tokura, Y., 2012. Observation of skyrmions in a multiferroic material. *Science*, 336(6078), pp.198-201.
- [28] Schulz, T., Ritz, R., Bauer, A., Halder, M., Wagner, M., Franz, C., Pfleiderer, C., Everschor, K., Garst, M. and Rosch, A., 2012. Emergent electrodynamics of skyrmions in a chiral magnet. *Nature Physics*, 8(4), pp.301-304.
- [29] Heinze, S., Von Bergmann, K., Menzel, M., Brede, J., Kubetzka, A., Wiesendanger, R., Bihlmayer, G. and Blügel, S., 2011. Spontaneous atomic-scale magnetic skyrmion lattice in two dimensions. *nature physics*, 7(9), pp.713-718.
- [30] Jiang, W., Chen, G., Liu, K., Zang, J., Te Velthuis, S.G. and Hoffmann, A., 2017. Skyrmions in magnetic multilayers. *Physics Reports*, 704, pp.1-49.
- [31] Neto, A. C., Guinea, F., Peres, N. M., Novoselov, K. S. and Geim, A. K., The electronic properties of graphene. *Rev. Mod. Phys.*, 81(1), p.109 (2009).
- [32] Okubo, T., Chung, S. and Kawamura, H. Multiple-q states and the skyrmion lattice of the triangular-lattice Heisenberg antiferromagnet under magnetic fields. *Phys. Rev. Lett.*, 108(1), p.017206 (2012).
- [33] Leonov, A. O. and Mostovoy, M., 2015. Multiply periodic states and isolated skyrmions in an anisotropic frustrated magnet. *Nature communications*, 6(1), pp.1-8.
- [34] Hayami, S., Ozawa, R. and Motome, Y., Effective bilinear-biquadratic model for noncoplanar ordering in itinerant magnets. *Phys. Rev. B*, 95(22), 224424 (2017).
- [35] Song, J. C., Samutpraphoot, P. and Levitov, L. S., Topological Bloch bands in graphene superlattices. *Proc. Natl. Acad. Sci.*, 112(35), 10879 (2015).
- [36] Bömerich T, Heinen L, Rosch A. Skyrmion and tetartion lattices in twisted bilayer graphene. *Phys. Rev. B*. 102(10):100408 (2020).
- [37] Khalaf, E., Chatterjee, S., Bultinck, N., Zaletel, M.P. and Vishwanath, A. Charged skyrmions and topological origin of superconductivity in magic-angle graphene. *Science advances*, 7(19), p.eabf5299 (2021).
- [38] Sondhi, S. L. and Karlhede, A. and Kivelson, S. A. and Rezayi, E. H., Skyrmions and the crossover from the integer to fractional quantum Hall effect at small Zeeman energies, *Phys. Rev. B*. 47.16419 (1993).
- [39] A. H. MacDonald, H. A. Fertig, and Luis Brey, Skyrmions without Sigma Models in Quantum Hall Ferromagnets, *Phys. Rev. Lett.* 76, 2153 (1996).
- [40] Fertig, H. A., Brey, L., Côté, R., MacDonald, A. H., Karlhede, A., and Sondhi, S. L., Hartree-Fock theory of Skyrmions in quantum Hall ferromagnets, *Phys. Rev. B* 55, 10671 (1997).
- [41] Nomura, K. and MacDonald, A.H. Quantum Hall ferromagnetism in graphene. *Phys. Rev. Lett.*, 96(25), p.256602. (2006).
- [42] Yang, K., Das Sarma, S., and MacDonald, A. H., Collective modes and skyrmion excitations in graphene $SU(4)$ quantum Hall ferromagnets, *Phys. Rev. B* 74, 075423 (2006).
- [43] Zhou, H., Polshyn, H., Taniguchi, T. et al. Solids of quantum Hall skyrmions in graphene. *Nat. Phys.* 16, 154–158 (2020).
- [44] Liu, X., Farahi, G., Chiu, C.L., Papic, Z., Watanabe, K., Taniguchi, T., Zaletel, M.P. and Yazdani, A. Visualizing broken symmetry and topological defects in a quantum Hall ferromagnet. *Science*, 375(6578) (2022).
- [45] Baskaran, G. and Anderson, P. W., Gauge theory of high-temperature superconductors and strongly correlated Fermi systems, *Phys. Rev. B*. 37.580 (1988).
- [46] Wiegmann, P. B., Superconductivity in strongly correlated electronic systems and confinement versus deconfinement phenomenon, *Phys. Rev. Lett.* 60.821 (1988).
- [47] Schulz, H. J., Effective action for strongly correlated fermions from functional integrals, *Phys. Rev. Lett.* 65.2462 (1990).
- [48] Ioffe, L. B. and Kalmeyer, V. and Wiegmann, P. B., Hall coefficient of the doped Mott insulator: A signature of parity violation, *Phys. Rev. B*. 43.1219 (1991).
- [49] Kenya Ohgushi, Shuichi Murakami, and Naoto Nagaosa. Spin anisotropy and quantum Hall effect in the kagomé lattice: Chiral spin state based on a ferromagnet. *Phys. Rev. B* 62, R6065 (2000).
- [50] Fujita, T., Jalil, M.B.A., Tan, S.G. and Murakami, S. Gauge fields in spintronics. *Journal of applied physics*, 110(12), p.17 (2011).
- [51] K. Hamamoto, M. Ezawa, and N. Nagaosa, Quantized topological Hall effect in skyrmion crystal, *Phys. Rev. B* 92, 115417 (2015).
- [52] Xiao, D., Yao, W. and Niu, Q. Valley-contrasting physics in graphene: magnetic moment and topological transport. *Phys. Rev. Lett.*, 99(23), p.236809 (2007).
- [53] Ref.[52] calculates the valley-dependent magnetization in a gapped Dirac band, arriving at an expression of the orbital magnetization (per spin) $M = \frac{e}{h} \int \frac{d^2 k}{(2\pi)^2} \mu \Omega(k) f(\epsilon_k)$, where the band Berry curvature $\Omega(k)$ is of opposite signs in the particle and hole bands, $f(\epsilon_k)$ is the Fermi-Dirac distribution. This result is established for a monolayer graphene with a staggered sublattice potential, however Ref.[52] argues that it is valid for a generic band with particle-hole symmetry. Applying this expression to our quadratic Dirac band model yields the orbital magnetization in Eq.(21).
- [54] See Online Supplement. In Sec. 1, we show microscopically that spin texture generates a pseudo magnetic field. This result directly leads to the $-M \cdot B$ coupling. In Sec. 2, we present a direct derivation of the orbital magnetization, Eq.(21), by a method that does not invoke Berry curvature.
- [55] Huberman, B.A. and Doniach, S. Melting of two-dimensional vortex lattices. *Phys. Rev. Lett.*, 43(13), p.950 (1979).
- [56] Fisher, D.S., Fisher, M.P. and Huse, D.A. Thermal fluctuations, quenched disorder, phase transitions, and transport in type-II superconductors. *Phys. Rev. B*, 43(1), 130 (1991).
- [57] Hu, J. and MacDonald, A.H. Two-dimensional vortex lattice melting. *Phys. Rev. Lett.*, 71(3), p.432 (1993).
- [58] Blatter, G., Feigel'man, M.V., Geshkenbein, V.B., Larkin, A.I. and Vinokur, V.M. Vortices in high-

temperature superconductors. Rev. Mod. Phys., 66(4), 1125 (1994).

- [59] Göbel, B., Mook, A., Henk, J. and Mertig, I. Unconventional topological Hall effect in skyrmion crystals caused by the topology of the lattice. Phys. Rev. B, 95(9), 094413 (2017).

Supplemental material for “Chiral Stoner magnetism in Dirac bands” by Z Dong and L Levitov

A. Spin-dependent pseudo magnetic field

In this section we substantiate the physical picture of a spin-dependent gauge field, described in the main text, by a microscopic derivation. In essence, spin of an electron moving through a spin texture is rotated in spin space. This spin rotation effect, arising due to an electron spin being locked to the local spin quantization axis and tracking it along the electron trajectory, is described by a spin-dependent geometric phase. This adiabatic regime in which the geometric phase picture applies occurs when the Stoner spin gap is large compared to $\hbar v/\ell$, where ℓ is the characteristic spatial lengthscale of the spin texture modulation and v is Fermi velocity.

Here we derive this result step by step starting from a microscopic Hamiltonian, Eq.(2) of the main text, finding that a spin texture gives rise to an effective gauge field whose flux density is associated with the spin chirality. In our analysis below, without loss of generality, we focus on spins in valley K and suppress the valley label. A spin texture is described by a position-dependent $\mathbf{S}(r)$. Our plan is to carry out an $SU(2)$ spin rotation to bring all the local spin polarization to the same orientation and, in this way, generate a Hamiltonian that features a spin-dependent pseudo-gauge-field term.

We start with a one-electron Hamiltonian in valley K , writing it in position space:

$$H(r) = \begin{pmatrix} D & \frac{(p_1 - ip_2)^2}{2m} \\ \frac{(p_1 + ip_2)^2}{2m} & -D \end{pmatrix} 1_S - h 1_L \mathbf{S}(r) \cdot \boldsymbol{\sigma} \quad (\text{S1})$$

where 1_S and 1_L are respectively the identity matrix in spin and sublattice variables. In the first term, $p_{1,2} = -i\partial_{1,2}$. The second term represents the effect of a position-dependent spin polarization arising after a Hubbard-Stratonovich transformation, see Eq.(5) of the main text. Next, we perform a position-dependent $SU(2)$ similarity transformation $T(r)$ on the Hamiltonian, such that it rotates all spins to the $+z$ direction:

$$T^\dagger(r)(\mathbf{S}(r) \cdot \boldsymbol{\sigma})T(r) = \sigma_3 \quad (\text{S2})$$

After the spin rotation, the Hamiltonian becomes

$$\begin{aligned} \tilde{H}(r) &= T^\dagger(r)H(r)T(r) \\ &= \begin{pmatrix} D & \frac{(\Pi_1 - i\Pi_2)^2}{2m} \\ \frac{(\Pi_1 + i\Pi_2)^2}{2m} & -D \end{pmatrix} 1_S - h 1_L \sigma_3 \end{aligned} \quad (\text{S3})$$

where

$$\begin{aligned} \Pi_\mu &= -iT^\dagger(r)\partial_\mu T(r) = p_\mu + A_\mu, \\ A_\mu &= -iT^\dagger(r)[\partial_\mu, T(r)], \quad \mu = 1, 2 \end{aligned}$$

Here $A_{1,2}$ are 2×2 matrices representing an $SU(2)$ gauge field, and the square brackets represent commutators. The quantities A_μ can be expressed in terms of Pauli matrices:

$$A_\mu = \sum_{i=1,2,3} a_{\mu,i} \sigma_i \quad (\text{S4})$$

In the adiabatic regime, where all spins track the spin-up or the spin-down states in rotated basis, the off-diagonal components $a_{\mu,1}$ and $a_{\mu,2}$ only contribute at a subleading order. We therefore keep only the diagonal σ_3 components in spin, finding

$$\Pi_\mu = p_\mu + a_\mu \sigma_3. \quad (\text{S5})$$

where from now on a_μ will be used as a shorthand for $a_{\mu,3}$. This result indicates that the spin-up and spin-down electrons, which describe the majority and minority spin in the original basis, see a $U(1)$ gauge field of opposite signs (here spin-up and spin-down refers to states in a rotated basis). After some algebra[1], one finds

$$a_\mu = \frac{1}{2}(1 - \cos \theta)\partial_\mu \phi \quad (\text{S6})$$

where θ and ϕ are the spherical polar and azimuthal angles measured with respect to the z axis introduced in Eq.(S2). The pseudo magnetic field B is then given by $B(\mathbf{x}) = \epsilon_{\mu\nu} \partial_\nu a_\mu = \nabla_x \times \mathbf{a}$. The result in Eq.(S6) indicates that the geometric phase picked up by an electron moving in the pseudo magnetic field $B(\mathbf{x})$ is equal to $1/2$ of the solid angle swept by the spin quantization axis, which is the result used in main text, Eq.(2).

B. Valley-dependent orbital magnetization in graphene bilayer

To gain more insight into the physics of the orbital magnetization, Eq.(21) of the main text, here we rederive this known result[5] by a method that does not explicitly use Berry curvature. Our plan is to calculate the orbital magnetization in an individual graphene valley using thermodynamic relation:

$$M_K = -\frac{\partial \Xi_K}{\partial B}, \quad (\text{S7})$$

where Ξ_K is the thermodynamic potential of electrons in this valley, defined as

$$\Xi_K = \sum_\alpha (\epsilon_\alpha - \mu) f(\epsilon_\alpha), \quad f(\epsilon) = \frac{1}{e^{\beta(\epsilon - \mu)} + 1} \quad (\text{S8})$$

where ϵ_α are the Landau level energies in the particle and hole bands, labeled by $\alpha = \{\pm, n\}$.

In order to obtain the magnetization at $B = 0$ we first calculate the Landau level energies ϵ_α and, by using the Euler-Maclaurin summation formula, extract the part of the sum over α in Eq.(S8) which is linear in B at small B . As we will see, the contribution linear in B is equal to that originating from the anomalous Landau levels reduced by a factor of two, as discussed below. We will end this section by discussing the general character of this result and its relation to the spectral flow.

The Landau level energies can be derived directly from the BBG Hamiltonian[3, 4]. For illustration, here we do it for a simplified form of the Hamiltonian involving no trigonal warping terms:

$$H_K(p) = \begin{pmatrix} D + \frac{p^2}{2m_0} + \frac{p^2}{2m_a} & -\frac{(p_1 - ip_2)^2}{2m} \\ -\frac{(p_1 + ip_2)^2}{2m} & -D - \frac{p^2}{2m_0} + \frac{p^2}{2m_a} \end{pmatrix} \quad (\text{S9})$$

Magnetic field can be incorporated in the Hamiltonian through the substitution $\mathbf{p} \rightarrow \mathbf{p} - \frac{e}{c}\mathbf{a}$. We will first carry out the analysis ignoring the terms $p^2/2m_0$ and $p^2/2m_a$. This is justified because these two terms are subleading for a realistic BBG band[3]. For the same reason we ignore the trigonal warping term (not shown in Eq.(S9)). To illustrate the generality of our results, we will subsequently present the analysis for the full Hamiltonian in Eq.(S9), finding that the quadratic terms $p^2/2m_0$ and $p^2/2m_a$ do not affect the result.

Next we consider the Landau levels formed in the presence of a B field, at first excluding the quadratic terms in the diagonal elements. As is well known, in each valley — K or K' — the Hamiltonian in Eq.(S9), with the quadratic terms excluded, in the presence of a magnetic field generates three groups of Landau levels: (i) a pair of anomalous Landau levels at the edges of the hole band for valley K and particle band for valley K' , and (ii) two sequences of Landau levels in the particle and hole bands that are related by particle-hole symmetry. The energies of these Landau levels in valley K can be written as [2]

$$\begin{aligned} \epsilon_{\pm,n} &= \epsilon_{\pm}(x_n) = \pm \sqrt{x_n^2 - \frac{1}{4}\hbar^2\omega_c^2 + D^2}, \quad n \geq 2, \\ \epsilon_{0,1} &= -D, \quad x_n = \hbar\omega_c \left(n - \frac{1}{2}\right), \end{aligned} \quad (\text{S10})$$

where $\omega_c = eB/m$ is the cyclotron frequency. For valley K' similar expressions arise, however the anomalous Landau levels are positioned at the particle band edge, $\epsilon_{0,1} = D$.

Accordingly, the thermodynamic potential Ξ_K in the presence of a B field is a sum of three contributions

$$\Xi_K = \Xi_+ + \Xi_- + \Xi_{01}, \quad (\text{S11})$$

where

$$\Xi_{\pm} = \frac{eB}{h} \sum_n (\epsilon_{\pm,n} - \mu) f(\epsilon_{\pm,n}), \quad (\text{S12})$$

$$\Xi_{01} = \frac{2eB}{h} (-D - \mu) f(-D), \quad (\text{S13})$$

with eB/h representing the numbers of electrons in each Landau level per unit area.

Magnetization is given by the linear ($O(B)$) term in $\Xi_K(B)$. The $O(B)$ contribution from the anomalous levels in each valley is already clearly written in Eq.(S13). To calculate the $O(B)$ contribution from Ξ_{\pm} we use the Euler-Maclaurin formula which approximates a sum by an integral. For the contribution of the particle band we have

$$\begin{aligned} \Xi_+ &= \frac{eB}{h} \left[\frac{1}{\hbar\omega_c} \int_{x_{n=2}}^{\infty} dx (\epsilon(x) - \mu) f(\epsilon(x)) \right. \\ &\quad \left. + \frac{1}{2} (\epsilon(x_{n=2}) - \mu) f(\epsilon(x_{n=2})) \right] + O(B^2), \end{aligned} \quad (\text{S14})$$

where $x_{n=2} = \frac{3}{2}\hbar\omega_c$, see Eq.(S10). Here we have used $\epsilon(\infty)f(\infty) = 0$. Working out the integral gives

$$\Xi_+ = -\frac{eB}{h} (D - \mu) f(D) + O(B^2). \quad (\text{S15})$$

Similarly, the $O(B)$ contribution of the lower-band Landau levels is given by

$$\Xi_- = -\frac{eB}{h} (-D - \mu) f(-D) + O(B^2). \quad (\text{S16})$$

After plugging Eqs. (S13), (S15) and (S16) into Eqs. (S7) and (S11), we arrive at

$$M_K(\mu) = \begin{cases} \frac{2eD}{2\pi\hbar}, & \mu > D \\ \frac{e(\mu+D)}{2\pi\hbar}, & -D < \mu < D \\ 0, & \mu < -D \end{cases}. \quad (\text{S17})$$

We note that this dependence differs by a constant shift by $\Delta M_K = \frac{eD}{2\pi\hbar}$ from the result in Eq.(21) of the main text that was inferred from the general expression for orbital magnetization obtained in Ref.[5]. This constant shift arises from the way the contribution of the deep-lying levels is cut off, which is different from the conventional way[5]. However, this difference is immaterial because the deep-lying states, due to their dubious valley character and identical occupancies for opposite spins, are not expected to affect physical observables.

Indeed, at the bottom of the graphene band the carrier states cannot be unambiguously identified with the K and K' valleys. Therefore the ambiguity arising from the cutoff is a matter of convention rather than a physical effect. Furthermore, the quantity that matters for the physics of interest is the difference of the contributions from the spin-up and spin-down bands, $\Delta M = M_{K,\uparrow} - M_{K,\downarrow}$. The bands for opposite spins are filled equally at the bottom, such that the contributions of the deep-lying states to $M_{K,\uparrow}$ and $M_{K,\downarrow}$ cancel each other.

The meaning of the resulting dependence $M_K(\mu)$, in which M_K is constant when the Fermi level lies within one of the bands, can be understood in terms of a spectral flow induced by a variation of B . Namely, the role of the Landau levels moving up and down is merely to cancel half of the contribution to magnetization M_K of the

anomalous Landau levels in the corresponding bands. As a result, there is no μ dependence when the Fermi level lies outside the gap. In that each anomalous level contributes a half of the ‘nominal value’ of a single Landau level. This contribution comes with a plus sign or a minus sign depending on whether an anomalous Landau level is present for the band and valley in question. The resulting dependence of orbital magnetization is identical for the K and K' valleys up to a sign reversal, $M_K(\mu) = -M_{K'}(\mu)$.

This analysis can be applied to a realistic model of biased Bernal bilayer graphene, where the band Hamiltonian takes a more complicated form[3]. Here we show that adding the two quadratic terms given in Eq.(S9), that were neglected temporarily, does not alter the result for $M_K(\mu)$.

The term $p^2/2m_a$ is an identity matrix in the sublattice variables. As a result, it merely shifts the energy eigen-

values without affecting the electron wavefunction that determines the orbital magnetization. Therefore, this term only affect the diamagnetic susceptibility but does not affect the magnetization at $B = 0$. Indeed, adding it in Eq.(S14) yields an $O(B^2)$ contribution to the thermodynamic potential, changing somewhat the diamagnetic susceptibility but not changing $M_K(\mu)$.

The term $p^2/2m_0$ has a σ_3 sublattice structure; therefore, this term does affect the wavefunctions. However, this term alone does not break the particle-hole symmetry. Also, this term does not affect the energy of the lowest Landau level in the particle band. As a result, the two conditions necessary for the reasoning above [from Eq.(S11) to Eq.(S16)] — the particle-hole symmetry and the two anomalous Landau levels — remain valid. Therefore, the result for magnetization remains unchanged.

-
- [1] K. Ohgushi, S. Murakami, and N. Nagaosa. Spin anisotropy and quantum Hall effect in the kagomé lattice: Chiral spin state based on a ferromagnet. *Phys. Rev. B* 62, R6065 (2000).
 - [2] Koshino, M. and Ando, T., Anomalous orbital magnetism in Dirac-electron systems: Role of pseudospin paramagnetism. *Phys. Rev. B*, 81(19), 195431 (2010).
 - [3] McCann, E. and Koshino, M. The electronic properties of bilayer graphene. *Reports on Progress in physics*, 76(5), p.056503 (2013).
 - [4] McCann, E. and Fal’ko, V.I., Landau-Level Degeneracy and Quantum Hall Effect in a Graphite Bilayer, *Phys-RevLett*.96.086805 (2006).
 - [5] Xiao, D., Yao, W. and Niu, Q. Valley-contrasting physics in graphene: magnetic moment and topological transport. *Phys. Rev. Lett.*, 99(23), p.236809 (2007).